International Journal of Non-Linear Mechanics 62 (2014) 12–22

Contents lists available at ScienceDirect

International Journal of Non-Linear Mechanics

journal homepage: www.elsevier.com/locate/nlm

A force-based frame finite element formulation for analysis of two- and three-layered composite beams with material non-linearity

Nima Khorsandnia [a,*], Hamid Valipour [a], Stephen Foster [a], Keith Crews [b]

[a] Centre for Infrastructure Engineering and Safety (CIES), School of Civil and Environmental Engineering, The University of New South Wales (UNSW), Sydney, Australia

[b] Centre for Built Infrastructure Research (CBIR), School of Civil and Environmental Engineering, University of Technology, Sydney (UTS), Australia

ARTICLE INFO

Article history:
Received 16 August 2013
Received in revised form
11 December 2013
Accepted 4 February 2014
Available online 12 February 2014

Keywords:
Deformable shear connection
Discrete non-linear spring
Frame FE model
Non-linear analysis
Timber–concrete composite

ABSTRACT

Presented in this paper is a formulation for an efficient frame finite element (FE) model for the non-linear analysis of timber–concrete and timber–timber composite structures. The element formulation is based on force interpolation concept and takes advantage of discrete non-linear springs to model the shear deformability between layers. The material non-linearity is taken into account, where the geometrical non-linearities are ignored. The developed formulation and analytical tool are employed to predict the ultimate loading capacity and load–deflection response of some experimental tests taken from the literature. The comparison between experimental results and numerical simulation shows the accuracy of the proposed model.

1. Introduction

The experimental programs for timber–concrete composite (TCC) and timber–timber composite (TTC) beams and floors are typically expensive and time consuming. Further, the empirical models directly derived from the test data have limited application as they are calibrated against limited sets of results with specific properties for timber, concrete and connection types. Accordingly, computer simulation and analytical modelling of structures, in particular finite element (FE) analysis, are considered a good alternative for assessing the loading capacity and predicting the short-term and long-term behaviour of TCC members under ultimate and service loads.

In terms of modelling the behaviour and analysis of composite structures such as TCC beams, many techniques have been developed that can be classified as analytical, semi-analytical or numerical. The analytical and semi-analytical models are typically derived from the solution of the governing differential equations for a simply-supported composite beam with linear elastic material and connection behaviour. Such models, however, cannot properly capture the non-linear behaviour of TCC beams and joints at the ultimate state of loading. Accordingly, for non-linear short- and long-term analysis of TCC members, a wide range of finite element (FE) models with different levels of accuracy and complexity have been developed. The existing FE models developed for analysis of TCC members can be classified as continuum-based [1–3] and discrete frame elements [4–6], which have different domains of applicability. The continuum-based FE models offer the versatility required for detailed analysis and modelling of the local effects, however, they are time-demanding from a computational point of view and are not efficient for investigating the global behaviour of structures, particularly when rigorous coupled procedures is required, such as long-term analysis of TCC. Frame models are a good compromise between accuracy and efficiency and they can capture the overall response of TCC and TTC beams under short- and long-term loads [4–6]. Accordingly, many authors have formulated various frame FE models to capture linear-elastic [7–11], linear-viscoelastic [12–14], materially non-linear [15–17] and geometrically non-linear [18–22] response of composite elements.

The main difference between the developed composite frame elements stems from the assumptions made for shear transfer and interaction between layers. Shear interaction between layers is provided by two main mechanisms; i.e. the mechanical connection and the friction due to contact on the interface. To the best of the authors' knowledge, no connection with full composite action has been reported for TCC and TTC floors. Existing connection systems including mechanical fasteners [23], glued and continuous mesh [24,25] and notched connections [25] can only provide a linear or

* Correspondence to: School of Civil and Environmental Engineering, The University of New South Wales (UNSW), Kensington, NSW 2052, Australia. Tel.: +61 2 9385 5656; fax: +61 2 9385 9747.
E-mail address: N.Khorsandnia@unsw.edu.au (N. Khorsandnia).

http://dx.doi.org/10.1016/j.ijnonlinmec.2014.02.001
0020-7462

non-linear partial shear interaction and the assumption of full composite action between the layers of TCC and TTC beams can lead to significant errors. In the deformable composite connections, two major phenomena can occur; slip between the layers along the beam length and uplift or separation in transvers direction. Uplift, however, is not normally significant compared to the interlayer slip, particularly at lower levels of deflections [26,27]. The shear interaction between the layers can be treated as continuous when the glued or mesh connectors are employed and/or there is a large number of connectors along the beam length. In such cases, the shear transfer mechanism is a relatively continuous phenomenon; whereas, for mechanical connectors (nails, SFS or coach screws) such an assumption cannot adequately represent the discrete nature of shear transfer [28]. On the other hand, using discrete connections (e.g. concentrated springs) can pose serious numerical challenges due to a jump in the shear load along the interface, particularly when non-linear analysis is required.

Many 1D frame FE models have been proposed that typically take advantage of a continuous shear transfer or slip function [4–6,21,29]. However, systematic formulation of a 1D composite frame element with discrete connections that can be specifically used for non-linear analysis of multi-layered TCC/TTC floors remains missing from the literature. Furthermore, the discrete model for typical TCC connections seems to be a better representative of the local behaviour, particularly where nails or screws are used for connecting the concrete slab to timber and, where discrete springs are incorporated, can readily accommodate the long-term behaviour of connections.

Various composite elements with displacement formulation have been proposed over the last three decades [4,17,19–21,28–36]. Less attention has been paid to the application of force-based and mixed formulations for development of non-linear 1D frame elements [15,18,37,38]. While displacement-based formulations are easier to be derived and implemented, force-based models or mixed formulations can generally provide more accurate results with fewer numbers of elements. This is because in force formulations the equilibrium equations are always satisfied in a strong sense [15,37]. In addition, 1D frame elements formulated based on force- or mixed-interpolation concepts are typically free of locking [37].

One-dimensional frame elements can be formulated based on Navier–Bernoulli hypothesis [7–11,19,20,31,33,34,36,38–40] or Timoshenko beam theory [18,21,28,29,32,34,35,40,41]. In the Navier–Bernoulli beam elements, the shear deformation is ignored and this assumption for beams with large depth-to-span (or shear-to-bending stiffness) ratios can lead to significant errors. Since the presence of shear strain in typical beams is inevitable, Timoshenko hypothesis can provide more accurate results, but do pose some kinematic complexities in the formulation. In TCC and TTC beams the depth-to-span ratios are usually less than 1/10 and, accordingly, the behaviour of such beams can be adequately represented by the Navier–Bernoulli hypothesis.

The application of composite theory can be extended to structural elements with more than two layers such as composite beams (steel–concrete, timber–concrete and steel–timber) retrofitted with FRP sheets, multi-layered timber floors and sandwich beams, just to mention a few [7,33–36,39,40,42]. With regard to the assumption adopted for shear transfer between the layers of a composite member, different formulations can be developed. In some of these formulations it is assumed that no shear slip takes place between the layers [7,36,42]. In the other formulations, a linear partial interaction between the layers is considered [33–35,39,40]. Typically, a continuous distribution of shear stress and/or slip is used for capturing the partial shear interaction between the layers and less attention has been paid to composite elements with lumped non-linear connections. In terms of material and connection behaviour, most of the developed composite models are based on linear elastic behaviour [7,33–35,39,40,42]; only a few studies have been devoted to formulations with material as well as connection non-linearities [36].

This paper focuses on development of a 1D frame FE model for short-term analysis of two- and/or three layered composite beams. The formulated element can take account of material non-linearities within different layers and it can be simply extended to multi-layered beams. The composite element is formulated within the framework of force interpolation using a modified fibre element; the accuracy and convergence characteristic of the proposed FE model for analyses of TCC and TTC beams is studied. The proposed element takes advantage of non-linear discrete springs (deformable connections) to capture the shear-slip between the layers, while the effect of friction and vertical partial interaction (uplift) between the layers are ignored. The developed model and the solution strategy are verified by comparing the numerical results with experimental data reported in the literature. The major features of this frame element are its simplicity and efficiency for non-linear analysis of layered composite beams, particularly design oriented parametric studies or coupled time-dependant analysis of TCC and/or TTC structures.

2. Element formulation

In this section, the formulation of two-layer composite beam is derived. The corresponding equations for the three-layer beam can be similarly obtained which are summarised in Appendix A.

2.1. Equilibrium equations

A plane composite frame element *AB* with two layers, four nodes and eight degrees of freedom (i.e. 2 horizontal and 1 vertical translations and 1 rotational DOFs at each end) is assumed (Fig. 1a). Also, at each end a non-linear spring with stiffness K is considered to capture the interlayer shear interaction. The load-slip behaviour of springs at each end can be different (K_A and K_B).

Fig. 1a shows the generalised nodal displacement and force vectors for the unrestrained element which are denoted by $\mathbf{q}=[\mathbf{q}_A|\mathbf{q}_B]^T$ and $\mathbf{Q}=[\mathbf{Q}_A|\mathbf{Q}_B]^T$, respectively. Regarding the domain of cantilever configuration (restrained system), the corresponding nodal generalised displacement and force vectors at end A are shown in Fig. 1b and denoted by $\mathbf{q}_A=[q_1\ q_2\ q_3\ q_4]^T$ and $\mathbf{Q}_A=[Q_1\ Q_2\ Q_3\ Q_4]^T$, respectively. The equilibrium equations for the arbitrary free body of length Ax (see Fig. 1c) can be expressed as

$$\mathbf{D}(x)=\mathbf{b}(x)\ \mathbf{Q}_A+\mathbf{K}_{CA}\ \mathbf{q}_A+\mathbf{D}_A^*(x)-\mathbf{D}_{cpA} \tag{1}$$

$$\mathbf{b}(x)=\begin{bmatrix}-1 & 0 & 0 & 0\\ 0 & x & -1 & 0\\ 0 & 0 & 0 & -1\end{bmatrix} \tag{2}$$

and

$$\mathbf{K}_{CA}=K_A\begin{bmatrix}1 & 0 & -H & -1\\ -H & 0 & H^2 & H\\ -1 & 0 & H & 1\end{bmatrix} \tag{3}$$

where $\mathbf{D}(x)=[N_1(x)\ M(x)\ N_2(x)]^T$ is the vector of section generalised forces, $\mathbf{b}(x)$ is the force interpolation matrix, $\mathbf{K}_{CA}$ is the matrix containing the stiffness of connector at end A, $\mathbf{D}_A^*(x)=[N_1^*(x)\ M^*(x)\ N_2^*(x)]^T$ is a vector of total section forces solely due to element loads at end A, $\mathbf{D}_{cpA}$ is a vector of section forces due to plastic slip in connector at end A and H represents the distance between the mid-planes of the layers.

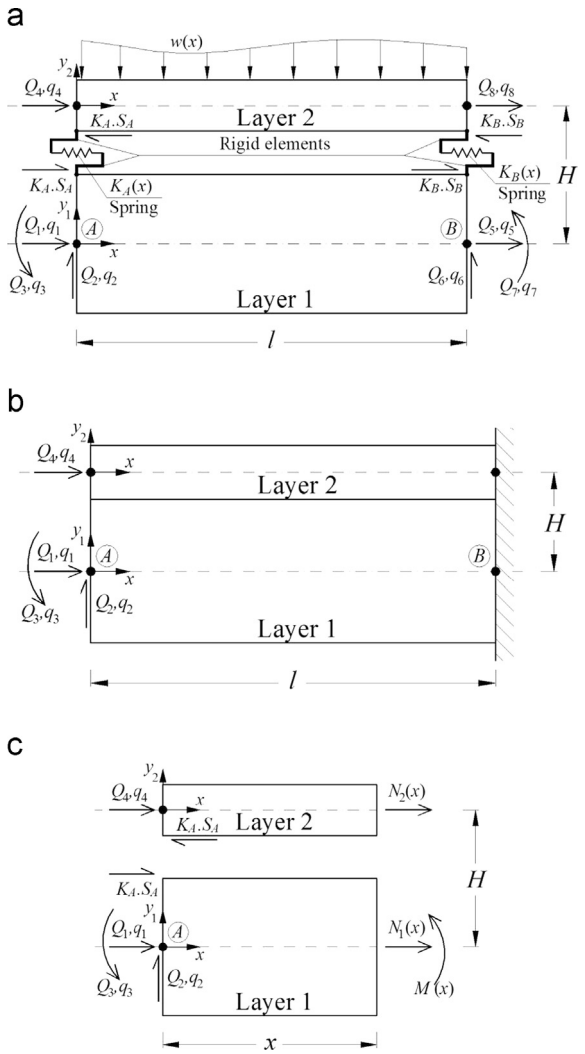

Fig. 1. (a) 2-node frame element *AB* with length *l*, (b) free body diagram of *Ax*, and (c) cantilever configuration of the element.

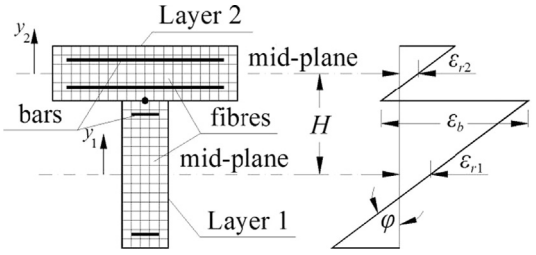

Fig. 2. Discretisation of a TCC or TTC section into fibres and distribution of strain over the depth of a section with partial interaction.

Equilibrium over the section yields

$$\mathbf{D}(x)=\begin{bmatrix}\int_{\Omega_1}\sigma_{x1}\,dA\\ -\int_{\Omega_1}\sigma_{x1}y_1\,dA-\int_{\Omega_2}\sigma_{x2}y_2 dA\\ \int_{\Omega_2}\sigma_{x2}\,dA\end{bmatrix} \tag{4}$$

where Ω_i denotes the layer i, y is the distance of the fibre (filament) from the mid-plane of the layer (see Fig. 2), σ_x is the total stress at the monitoring point within section x along the member axis. The subscripts 1 and 2 denote the component of the corresponding layer.

2.2. Compatibility equations

Assuming deformable shear interaction between the layers and adopting Navier–Bernoulli hypothesis for each layer separately can establish the compatibility requirement (see Fig. 2) and lead to

$$\varepsilon_{xi}=\varepsilon_{ri}-y_i\varphi \quad (i=1,\ 2) \tag{5}$$

and

$$\varepsilon_b=(\varepsilon_{r2}-\varepsilon_{r1})-H\varphi \tag{6}$$

where ε_{xi} denotes the total longitudinal strain at the monitoring points (fibres), ε_{ri} is the section axial strain at the mid-plane of the layer Ω_i, φ denotes the total curvature of section, ε_b is the slip strain and subscript i denotes the component of a composite section ($i=1$ for the layer 1 and $i=2$ for the layer 2).

2.3. Material constitutive law

Decomposing the total strain (ε_{xi}) into its elastic (ε_{exi}) and plastic (ε_{pxi}) components, the constitutive law in the framework of total secant approach in x–x direction can be expressed by

$$\sigma_{xi}=E_{ei}\varepsilon_{exi}=E_{ei}\ (\varepsilon_{xi}-\varepsilon_{pxi}) \quad (i=1,\ 2) \tag{7}$$

where E_{ei} is the elastic secant modulus of the theoretical unloading curve (Fig. 3) and is a function of the stress and strain components at the integration point under consideration.

2.4. Element formulation

Introducing the identities

$$k_{i_{11}}=\int_{\Omega_i}E_{ei}\ dA \tag{8a}$$

$$k_{i_{12}}=-\int_{\Omega_i}y_iE_{ei}\ dA \tag{8b}$$

$$k_{i_{22}}=-\int_{\Omega_i}y_i^2E_{ei}\ dA \tag{8c}$$

$$N_{pi}(x)=-\int_{\Omega_i}E_{ei}\varepsilon_{pxi}\ dA \tag{8d}$$

$$M_{pi}(x)=\int_{\Omega_i}y_iE_{ei}\ \varepsilon_{pxi}\ dA \tag{8e}$$

and substituting Eqs. (5) and (7) into Eq. (4) gives

$$\mathbf{D}(x)=\mathbf{k}_s(x)\mathbf{d}(x)+\mathbf{D}_p(x) \tag{9}$$

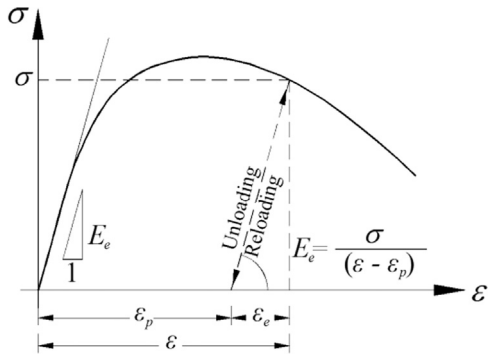

Fig. 3. Total secant concept within a uni-axial model including plastic strains.

in which

$$\mathbf{k}_s(x)=\begin{bmatrix} k_{1_{11}} & k_{1_{12}} & 0 \\ k_{1_{12}} & k_{1_{22}}+k_{2_{22}} & k_{2_{12}} \\ 0 & k_{2_{12}} & k_{2_{11}} \end{bmatrix} \tag{10}$$

and

$$\mathbf{D}_p(x)=\begin{bmatrix} N_{p1}(x) & M_{p1}(x)+M_{p2}(x) & N_{p2}(x) \end{bmatrix}^T \tag{11}$$

where $\mathbf{k}_s(x)$ is the secant stiffness matrix of the cross-section, $\mathbf{D}_p(x)$ is the residual plastic force vector for the section, and $\mathbf{d}(x)=[\varepsilon_{r1}\ \varphi\ \varepsilon_{r2}]^T$ is the section generalised strain vector. The flexibility matrix of the section $\mathbf{f}_s(x)$ is obtained by inverting the section stiffness matrix, and so Eq. (9) can be rearranged as

$$\mathbf{d}(x)=\mathbf{f}_s(x)\{\mathbf{D}(x)-\mathbf{D}_p(x)\} \tag{12}$$

Adopting the small strain assumption in conjunction with Navier–Bernoulli beam theory and applying the principle of virtual work for the cantilever configuration *AB* shown in Fig. 1b, leads to the compatibility condition

$$\mathbf{q}_A=\int_0^l \mathbf{b}^T(x)\mathbf{d}(x)\,dx \tag{13}$$

Submitting Eqs. (1) and (12) into Eq. (13) gives

$$(\mathbf{I}-\mathbf{B}_A)\mathbf{q}_A=\mathbf{F}_{AA}\mathbf{Q}_A+\mathbf{q}_A^*-\mathbf{q}_{pA}-\mathbf{q}_{cpA} \tag{14}$$

where

$$\mathbf{F}_{AA}=\int_0^l \mathbf{b}^T(x)\mathbf{f}_s(x)\mathbf{b}(x)\,dx \tag{15}$$

$$\mathbf{B}_A=\left\{\int_0^l \mathbf{b}^T(x)\mathbf{f}_s(x)\,dx\right\}\mathrm{K}_{CA} \tag{16}$$

$$\mathbf{q}_A^*=\int_0^l \mathbf{b}^T(x)\mathbf{f}_s(x)\mathbf{D}_A^*(x)\,dx \tag{17}$$

$$\mathbf{q}_{pA}=\int_0^l \mathbf{b}^T(x)\mathbf{f}_s(x)\mathbf{D}_p(x)\,dx \tag{18}$$

$$\mathbf{q}_{cpA}=\int_0^l \mathbf{b}^T(x)\mathbf{f}_s(x)\mathbf{D}_{cpA}\,dx \tag{19}$$

In Eqs. (14)–(19), $\mathbf{B}_A$ is the stiffness matrix due to stiffness of the connector at end *A*, $\mathbf{q}_A$ is the generalised deformation vector at end *A* for the cantilever configuration, $\mathbf{q}_A^*$ represents the vector of the nodal generalised deformations due to element loads at end *A*, $\mathbf{q}_{pA}$ is the vector of the nodal generalised plastic deformations at end *A*, $\mathbf{q}_{cpA}$ is the vector of the nodal generalised deformations due to plastic slip in the connector at end *A* and $\mathbf{I}$ is a 4×4 identity matrix.

Pre-multiplying both sides of Eq. (14) by $\mathbf{K}_{AA}=[\mathbf{F}_{AA}]^{-1}$, yields

$$\mathbf{K}_{AA}^e\mathbf{q}_A=\mathbf{Q}_A+\mathbf{Q}_A^*-\mathbf{Q}_{pA}-\mathbf{Q}_{cpA} \tag{20}$$

in which $\mathbf{K}_{AA}^e=\mathbf{K}_{AA}(\mathbf{I}-\mathbf{B}_A)$ represents the stiffness sub-matrix of end *A* for the element *AB* shown in Fig. 1a, $\mathbf{Q}_A$ is the generalised force vector at end *A*, $\mathbf{Q}_A^*$ and $\mathbf{Q}_{pA}$ denote the nodal generalised force vector due to element loads and vector of the nodal generalised plastic forces at end *A*, respectively, and $\mathbf{Q}_{cpA}$ represents the vector of the nodal generalised forces due to plastic slip in the connector at end *A*.

The global equilibrium of cantilever configuration for element *AB* shown in Fig. 1b gives

$$\mathbf{Q}_B=\mathbf{\Gamma}\mathbf{Q}_A+\mathbf{T}\mathbf{K}_{CA}\mathbf{q}_A-\mathbf{T}\mathbf{D}_{cpA} \tag{21}$$

$$\mathbf{\Gamma}=\begin{bmatrix} -1 & 0 & 0 & 0 \\ 0 & -1 & 0 & 0 \\ 0 & l & -1 & 0 \\ 0 & 0 & 0 & -1 \end{bmatrix} \tag{22}$$

$$\mathbf{T}=\begin{bmatrix} 1 & 0 & 0 \\ 0 & 0 & 0 \\ 0 & 1 & 0 \\ 0 & 0 & 1 \end{bmatrix} \tag{23}$$

where $\mathbf{\Gamma}$ and $\mathbf{T}$ are the transformation matrices. Pre-multiplying Eq. (20) by $\mathbf{\Gamma}$ and then subtracting it from Eq. (21) gives

$$\mathbf{K}_{BA}^e\mathbf{q}_A=\mathbf{Q}_B+\mathbf{\Gamma}\mathbf{Q}_A^*-\mathbf{\Gamma}\mathbf{Q}_{pA} \tag{24}$$

in which $\mathbf{K}_{BA}^e=\mathbf{\Gamma}\mathbf{K}_{AA}^e+\mathbf{T}\mathbf{K}_{CA}$.

Solving the equilibrium equations for the cantilever frame element clamped at end *A* and subjected to nodal forces at end *B* yields similar equations as follows:

$$\mathbf{K}_{AB}^e\mathbf{q}_B=\mathbf{Q}_A+\mathbf{\Gamma}^{-1}\mathbf{Q}_B^*-\mathbf{\Gamma}^{-1}\mathbf{Q}_{pB} \tag{25}$$

$$\mathbf{K}_{BB}^e\mathbf{q}_B=\mathbf{Q}_B+\mathbf{Q}_B^*-\mathbf{Q}_{pB}-\mathbf{Q}_{cpB} \tag{26}$$

where

$$\mathbf{K}_{AB}^e=\mathbf{K}_{AA}\mathbf{\Gamma}^T(\mathbf{I}+\mathbf{B}_B)+\mathbf{T}\mathbf{K}_{CB} \tag{27}$$

$$\mathbf{K}_{BB}^e=\mathbf{\Gamma}\mathbf{K}_{AA}\mathbf{\Gamma}^T(\mathbf{I}+\mathbf{B}_B) \tag{28}$$

$$\mathbf{Q}_B^*=\mathbf{\Gamma}\ \mathbf{K}_{AA}\ \mathbf{q}_B^*=\mathbf{\Gamma}\ \mathbf{K}_{AA}\ \int_0^l \mathbf{b}^T(x)\,\mathbf{f}_s(x)\,\mathbf{D}_B^*(x)\,dx \tag{29}$$

$$\mathbf{Q}_{pB}=\mathbf{\Gamma}\mathbf{Q}_{pA} \tag{30}$$

$$\mathbf{Q}_{cpB}=\mathbf{\Gamma}\mathbf{K}_{AA}\mathbf{q}_{cpB}=\mathbf{\Gamma}\mathbf{K}_{AA}\int_0^l \mathbf{b}^T(x)\mathbf{f}_s(x)\mathbf{D}_{cpB}\,dx \tag{31}$$

and

$$\mathbf{B}_B=\mathbf{\Gamma}^{-T}\left\{\int_0^l \mathbf{b}^T(x)\mathbf{f}_s(x)dx\right\}\mathbf{K}_{CB} \tag{32}$$

$$\mathbf{K}_{CB}=K_B\begin{bmatrix} 1 & 0 & -H & -1 \\ -H & 0 & H^2 & H \\ -1 & 0 & H & 1 \end{bmatrix}. \tag{33}$$

In the proposed formulation, the effect of different types of element loads including constant and trapezoidal distributed loads are reflected in the sectional force vectors, i.e. $\mathbf{D}_A^*(x)$ and $\mathbf{D}_B^*(x)$. For example, if a constant horizontal and a vertical uniform distributed load (i.e. w_x and w_y) are applied on the element, then the corresponding sectional force vectors at end *A* and *B* can be obtained from

$$\mathbf{D}_A^*(x)=\begin{bmatrix} -w_x x & w_y\frac{x^2}{2} & 0 \end{bmatrix}^T \tag{34}$$

$$\mathbf{D}_B^*(x)=\begin{bmatrix} w_x(l-x) & w_y\frac{(l-x)^2}{2} & 0 \end{bmatrix}^T \tag{35}$$

Finally, the total stiffness matrix of the element can be generated by assembling the sub-matrices of ends *A* and *B* and using the equilibrium equation for the undeformed cantilever configuration (without rigid body motion). Accordingly, Eqs. (20), (24)–(26) can be recast into the following matrix form:

$$\begin{bmatrix} \mathbf{K}_{AA}^e & \mathbf{K}_{AB}^e \\ \mathbf{K}_{BA}^e & \mathbf{K}_{BB}^e \end{bmatrix}\begin{bmatrix} \mathbf{q}_A \\ \mathbf{q}_B \end{bmatrix}=\begin{bmatrix} \mathbf{Q}_A \\ \mathbf{Q}_B \end{bmatrix}+\begin{bmatrix} \mathbf{Q}_A^* \\ \mathbf{Q}_B^* \end{bmatrix}-\begin{bmatrix} \mathbf{Q}_{pA} \\ \mathbf{\Gamma}\mathbf{Q}_{pA} \end{bmatrix}-\begin{bmatrix} \mathbf{Q}_{cpA} \\ \mathbf{Q}_{cpB} \end{bmatrix} \tag{36}$$

Eq. (36) is the governing equation of the element and can be solved using a direct iteration solution scheme [37,43]. Following a similar approach, the composite beam with 3 layers is formulated and the derived matrices are given in Appendix A.

It should be emphasised that in the proposed formulation, the diagonal sub-matrices $\mathbf{K}^e_{AA}$and $\mathbf{K}^e_{BB}$ were derived by applying the principle of virtual work for cantilever configurations, which are, respectively, fixed at ends *B* and *A*. Sub-matrices $\mathbf{K}^e_{AB}$, $\mathbf{K}^e_{BA}$ were obtained with respect to $\mathbf{K}^e_{AA}$and $\mathbf{K}^e_{BB}$ by using equilibrium equation. Alternatively, in some of the force-based formulation the sub-matrix $\mathbf{K}^e_{AA}$ is derived from principle of virtual work and the other three sub-matrices, i.e. $\mathbf{K}^e_{AB}$, $\mathbf{K}^e_{BA}$ and $\mathbf{K}^e_{BB}$, are related to $\mathbf{K}^e_{AA}$ by applying the equilibrium equations for the undeformed configuration (element without rigid body modes) [43].

3. Adopted material model

Typical in the fibre element models, the Navier–Bernoulli beam hypothesis is adopted and the effect of shear deformations on the non-linear response of material is neglected. Accordingly, a uniaxial constitutive law can adequately capture the non-linear behaviour of each component in the direction parallel to grain (along the beam axis).

3.1. Timber

Most of the proposed stress–strain relationships for timber under tension and compression are almost linear. Among the various available uniaxial constitutive laws for timber in compression [44], Glos's stress–strain law [45], originally developed for small clear timber specimens, is adopted in this study (Fig. 4). This relationship is given by

$$\sigma = \begin{cases} \dfrac{\varepsilon+\alpha_1\varepsilon^n}{\alpha_2+\alpha_3\varepsilon+\alpha_4\varepsilon^n} & \text{for} \quad -\varepsilon_{cu}\le\varepsilon\le 0 \\ 0 & \text{for} \quad \varepsilon<-\varepsilon_{cu} \end{cases} \tag{37}$$

where

$$\alpha_1 = \frac{100 f_{cy}}{(n-1)E_c\varepsilon_{c0}^{(n-1)}(1-f_{cy}/f_{cu})}, \quad f_{cy}\le f_{cu}-1 \ \text{(MPa)} \tag{38a}$$

$$\alpha_2 = \frac{1}{E_c} \tag{38b}$$

$$\alpha_3 = \frac{1}{f_{cu}} - \frac{n}{(n-1)E_c\varepsilon_{c0}} \tag{38c}$$

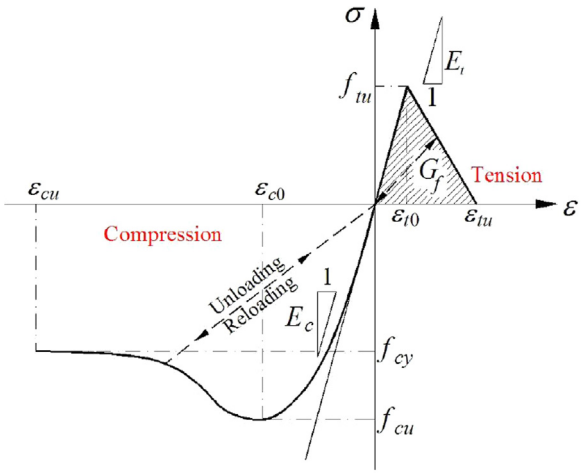

Fig. 4. Schematic outline of the adopted stress–strain relationship for timber.

$$\alpha_4 = \frac{\alpha_1}{f_{cy}} \tag{38d}$$

and f_{cu} and ε_{c0} are the ultimate compressive strength and corresponding strain, respectively, f_{cy} is the residual stress, E_c is the initial elastic modulus of timber in compression and n is a shape parameter which controls the curvature (see Fig. 4). According to this model, there is non-linearity in compression particularly near the ultimate and post peak stresses. The typical values adopted for the input parameters in the Glos [45] model are: $f_{cy}=0.8f_{cu}$, $\varepsilon_{c0}=0.004-0.012$ and $\varepsilon_{cu}\approx 3\varepsilon_{c0}$. In this paper, $\varepsilon_{c0}=0.004$ and $\varepsilon_{cu}=0.012$ are taken unless otherwise mentioned.

The behaviour of timber in tension follows a linear elastic part up to tensile strength, f_{tu}, with a modulus of elasticity, E_t. After the peak strength is reached, the material softens linearly (see Fig. 4). The slope of the softening branch is characterised and adjusted by assuming a constant fracture energy density G_f (e.g. $\varepsilon_{tu}=2\varepsilon_{t0}$) that serves as a localisation limiter. Moreover, as shown in Fig. 4 a damage model with no plastic strain is adopted for timber in this study.

3.2. Concrete

In the developed 1D frame fibre element model, a uniaxial stress–strain relationship based on the CEB-FIP model code 1990 [46] is used for ascending part of the concrete under compression follows by a linear descending part after maximum compressive strength. A linear elastic-quasi brittle failure model with an exponential softening curve is employed for tension (Fig. 5). In this paper, the strain corresponding with maximum stress for compressive concrete is taken as $\varepsilon_{c0}=0.002$ and the ultimate strain of concrete is taken as $\varepsilon_{cu}=0.01$ (Fig. 5), unless otherwise mentioned. For the unloading/reloading regime, a damage model with no plastic strain is adopted (Fig. 5).

3.3. Steel

A linear elastic–perfectly plastic-hardening model is adopted for steel bars (Fig. 6). The yielding stress, f_y, the ultimate stress, f_u, the initial elastic modulus, E_{st}, and the strain hardening modulus, E_{sh}, are taken as 400 MPa, 600 MPa, 200 GPa and 1 GPa, respectively, unless otherwise mentioned, and for unloading–reloading regime a modulus equal to initial elastic modulus is employed (see Fig. 6).

3.4. Connection

In the model, a non-linear discrete spring at each end is considered to transfer the horizontal shear between layers.

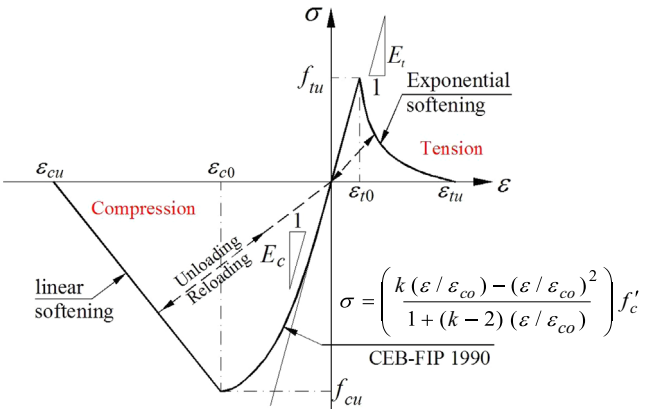

Fig. 5. Schematic outline of the adopted stress–strain relationship for concrete.

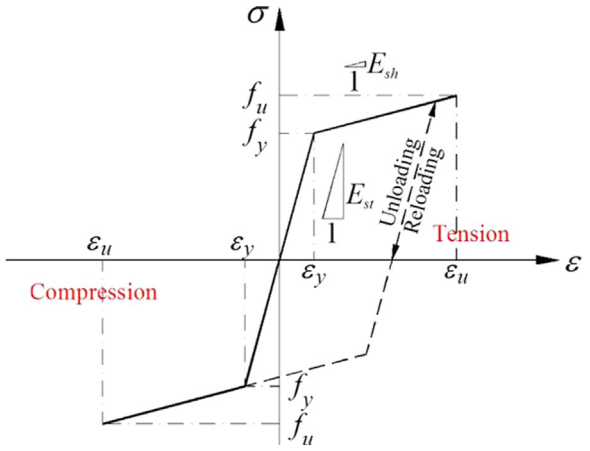

Fig. 6. Schematic outline of the adopted stress–strain relationship for steel.

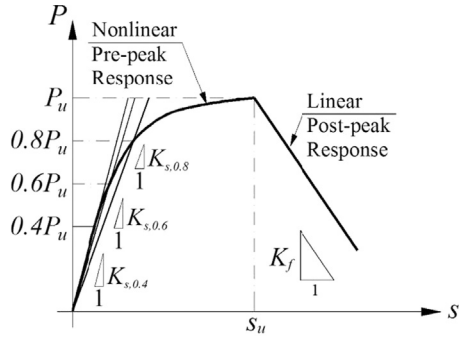

Fig. 7. Schematic outline of the adopted load–slip relationship for connection.

The stiffness and load–slip behaviour of these springs can be different (Fig. 1a). In TCC and TTC beams, the load–slip response can be obtained from push-out test. For different types of connections, various tests have been reported in the literature and different models have been proposed [25]. The proposed models represent the ascending (pre-peak) part as well as the descending (post-peak) part of the load–slip relationship. The ascending part of the load–slip often follows a non-linear curve, whereas the descending part can be adequately represented by a linear function (see Fig. 7). The main characteristics of connections are the slip, s_u, that corresponds to ultimate load, P_u, the slip modulus for serviceability, $K_{s,0.4}$, at ultimate, $K_{s,0.6}$, and near collapse, $K_{s,0.8}$, ranges, and softening stiffness (K_f) (see Fig. 7).

4. Error estimation

The accuracy and convergence characteristic of the proposed FE model is evaluated in this part by analysing a cantilever configuration subjected to a point load P (see Fig. 8) and reporting the error in the vertical displacement at end A (q_2) and the errors in the horizontal force and bending moment reactions at end B (Q_5 and Q_7) with respect to number of elements in Figs. 9 and 10. Based on the results obtained, the error of horizontal displacements (q_1 and q_4), rotation (q_3) and vertical reaction (Q_6) are always zero and the error of Q_8 is equal in magnitude and opposite sign to Q_5. Moreover, there is no error in all the displacements and forces when the spring stiffness (K_s) is zero, and the maximum error occurs when the spring stiffness tends to infinity. Therefore, the error varies from zero to a specific limit for different values of K_s/K_b (i.e. spring to beam stiffness). The error for vertical displacement (q_2), horizontal reaction (Q_5) and moment reaction (Q_7)

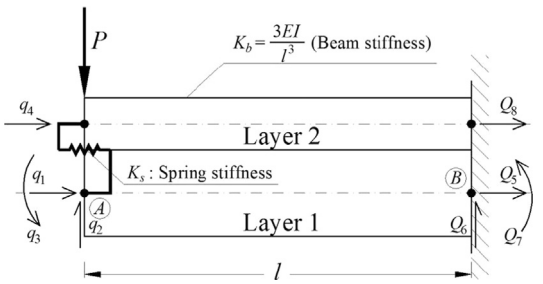

Fig. 8. Outline of the cantilever configuration adopted for error estimation and investigating the convergence characteristic of developed frame element.

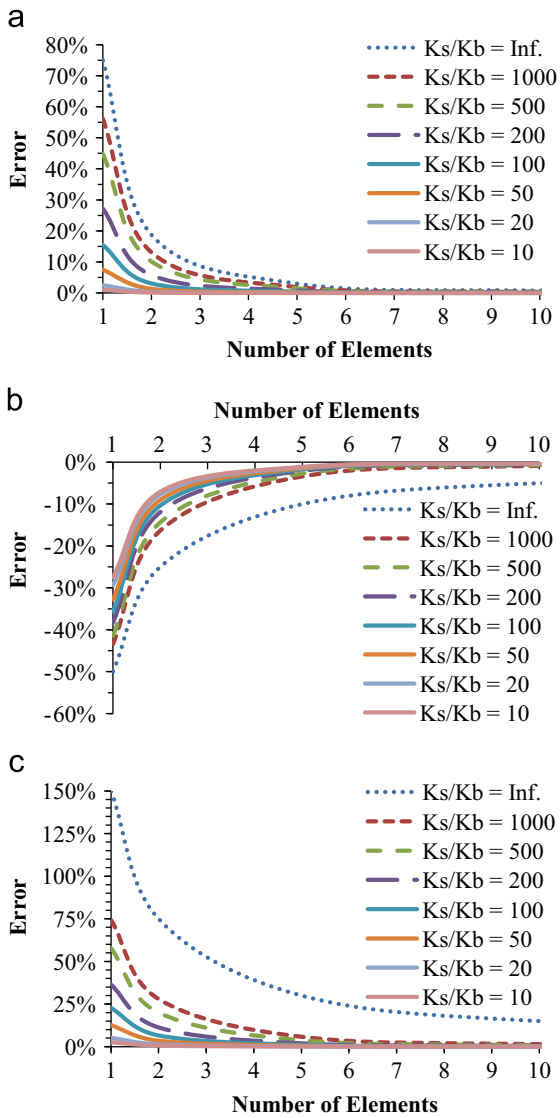

Fig. 9. Error versus number of elements for different values of K_s/K_b in (a) vertical displacement (q_2), (b) horizontal reaction (Q_5), and (c) moment reaction (Q_7).

versus number of elements for different values of K_s/K_b are shown in Fig. 9. The maximum error when $K_s \to \infty$ is also shown in Fig. 10. The high convergence rate of the developed formulation is shown in Fig. 10 with errors in displacements much less than the errors of forces. The typical stiffness of mechanical connectors in TCC/TTC beams is usually less than $200K_b$, for the maximum 2.0 m element length investigated. Accordingly the developed formulation can adequately capture the behaviour of TCC or TTC beams with low level of composite efficiency and for TCC or TTC beams with close

to full-composite action, increasing the number of elements (6–10 elements) can provide sufficiently accurate results.

5. Verification of developed model

The performance of the FE model developed in this paper is validated through experimentally measured data and numerically predicted short-term response. The considered experimental data are related to simply-supported two- and three-layered composite beams subjected to 4-point bending tests, as shown in Fig. 11.

5.1. Two-layered composite beams

A test conducted at University of Florance (Italy) by Ceccotti et al. [24] is analysed in this example. The TCC beam is 6 m long and comprised of two separate timber joists connected with glued-in connections to a concrete slab on top. The beam was first subjected to long-term loads for 5 years in out-door conditions and then was loaded to failure to investigate the short-term behaviour. The vertical deflection at midspan, maximum slips over the supports and strains at midspan were recorded during the tests; these values are used to validate the developed FE model. The beam was modelled using three elements. The dimensions and geometrical properties of the beam are reported in Table 1. The load–slip relationship of the connection was taken from Ceccotti et al. [47] and the maximum ratio of connection initial stiffness over beam stiffness (K_s/K_b) is 0.16. Furthermore, the mechanical properties of the materials taken from the test data are given in Table 2.

The comparison between experimentally measured data and numerically predicted results from this study and FE model developed by Ceccotti et al. [47], as well as full-composite and no-composite responses, are shown in Figs. 12–16. Figs. 12–16 display the total load versus midspan deflection, maximum slip over the supports, upper and lower timber stress at midspan, upper concrete stress and distance of the neutral axis from the upper timber fibre, respectively. Based on the results obtained, the TCC beam exhibits partial-composite behaviour with almost linear response up to failure; however, there is some non-linearity near the collapse load particularly in load–slip response (see Fig. 13). Overall, the FE model is demonstrated to adequately capture the response of the TCC beams. Some of the discrepancies between the

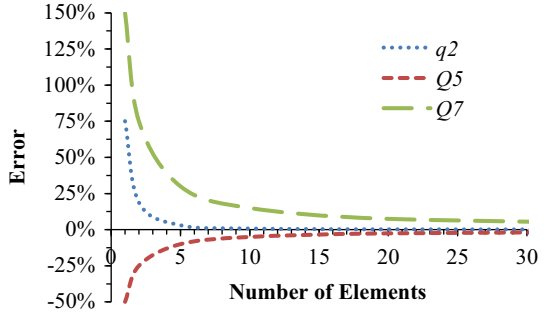

Fig. 10. Maximum error versus number of elements for vertical displacement (q_2), horizontal reaction (Q_5), and bending moment reaction (Q_7).

Table 2
Adopted material properties of TCC beam tested by Ceccotti et al. [24].

Material	E (GPa)	f_{cu} (MPa)	f_{tu} (MPa)	G_f (MPa)	ε_{c0} (%)	f_y (MPa)	f_u (MPa)
Timber	10	40	29	0.084	0.4	–	–
Concrete	30.4	30.4	3.3	–	0.2	–	–
Steel	200	–	–	–	–	400	600

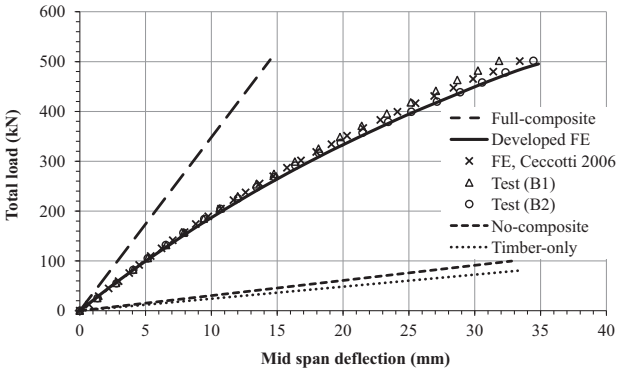

Fig. 12. Total load versus midspan deflection of TCC beam tested by Ceccotti et al. [24].

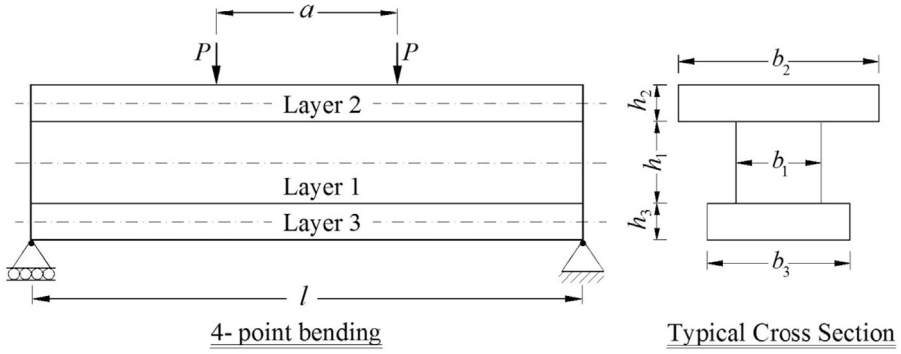

Fig. 11. Schematic outline of the 4-point bending test and typical composite cross-section used in the verification study.

Table 1
Dimensions and geometrical properties of TCC beam tested by Ceccotti et al. [24].

l (m)	a (m)	Timber	Concrete		Connection		
		$b_1 \times h_1$ (mm)	$b_2 \times h_2$ (mm)	Bar (mm^2)	No.	Type	Load–slip relationship
5.7	1.8	(2 ×)125 × 500	1500 × 100	5ø6@300 Top	19 × 2	Glued re-bar	$P=40(1-e^{-0.7s})^{0.9}$

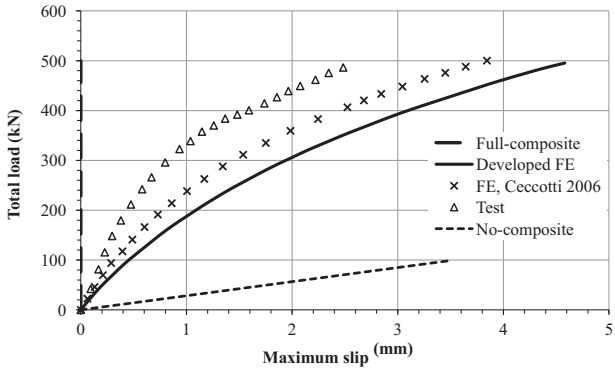

Fig. 13. Total load versus slip over the supports for TCC beam tested by Ceccotti et al. [24].

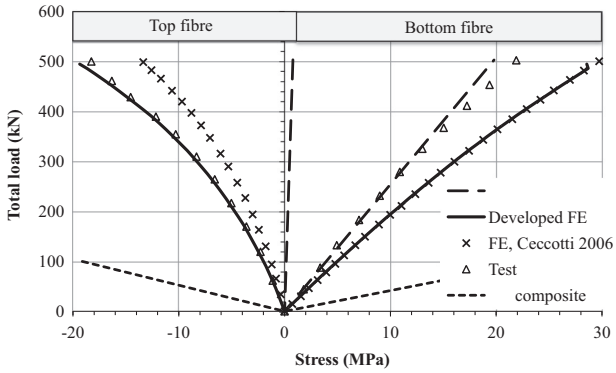

Fig. 14. Total load versus upper (left) and lower (right) timber stress at midspan of TCC beam tested by Ceccotti et al. [24].

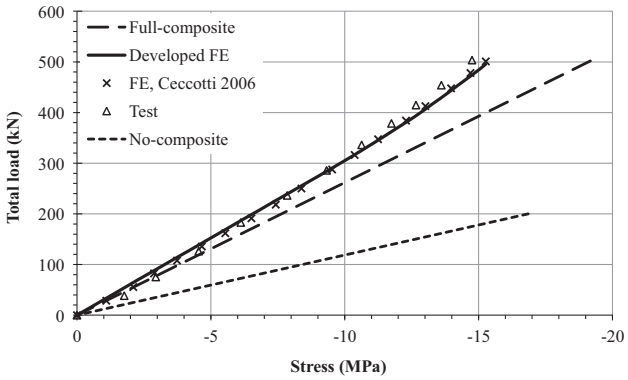

Fig. 15. Total load versus concrete stress at midspan of TCC beam tested by Ceccotti et al. [24].

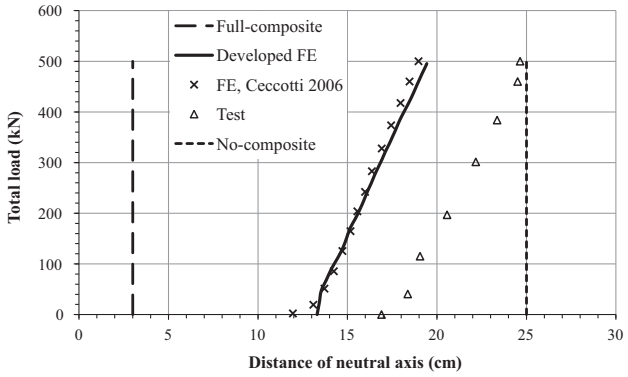

Fig. 16. Total load versus distance of the neutral axis from the upper timber fibre of TCC beam tested by Ceccotti et al. [24].

experimental results and the numerical predictions (see Figs. 13 and 16) can be attributed to the residual deformations occurred during the long-term test on TCC beams. Also, the poor correlation between some of the experimental and numerical results can be attributed to the variability in mechanical properties of timber and connections, which are highly sensitive to environmental conditions (e.g. relative humidity).

The comparison between the proposed frame element and the FE model developed by Ceccotti et al. [47] shows that the overal accuracy of both FE models are similar, and in one case the FE model developed in this study displays generally better results (see Fig. 14). Furthermore, the ultimate loading capacity (P_u) and corresponding ultimate deflection (δ_u) of the TCC beam predicted by FE models are compared with experimental results in Table 3. It is observed that the frame FE model developed in this study can capture the short-term behaviour of two-layer timber–concrete composite beams with reasonable accuracy.

5.2. Three-layered composite beams

For verification of three-layered composite beams, two different sets of results from the studies of Zabihi et al. [48] and Ferrier et al. [49] are used. In Zabihi et al. [48], timber–timber full-scale composite beams were constructed and tested under short-term loads to study the performance of built-up LVL timber beams. The built-up cross-section of the beams in Zabihi et al. [48] tests comprises a wide spread top flange, two webs as well as two bottom flanges connected to the webs with different dimensions (see Table 4). The composite beam tested by Ferrier et al. [49] is a rectangular glulam beam strengthened by ultra-high performance concrete (reinforced with steel or FRP) at the bottom and top of a timber joist. Amongst various tests conducted in this study, the beam BLCHP-S-130-5m is chosen, which has a 5.1 m span with steel reinforcement in the bottom concrete element. The dimensions and geometrical properties of the beams are reported in Table 4 and the material properties of the beams, taken from Ferrier et al. [50], for different layers are given in Table 5.

Fig. 17 shows the load versus midspan deflection of the TTC beams tested by Zabihi et al. [48]. The results are mostly linear up to failure point, which is typical of timber beams, and there is an excellent agreement between experimental and numerical results in terms of beam stiffness. Further, the strain profile over the beam depth at different load levels is shown in Fig. 18, which demonstrates the near linear distribution of the strain over the section depth and validity of the Navier–Bernoulli hypothesis. Also, the total load versus midspan deflection of the hybrid beam tested by Ferrier et al. [49] is displayed in Fig. 19. There are some non-linearities in the beam load–deflection response particularly near the collapse load, which can be accurately captured by the developed FE model.

The experimental and numerical results for the ultimate loading capacity, and corresponding ultimate deflection, for the analysed composite beams of Zabihi et al. [48] and Ferrier et al. [49] are given in Table 6. A good correlation between experimental results and the developed FE model is observed and demonstrates the adequacy of

Table 3
Ultimate loading capacity (P_u) and corresponding ultimate deflection (δ_u) of TCC beam tested by Ceccotti et al. [24].

Method	P_u (kN)	δ_u (mm)	P_u(FE)/P_u(test)	δ_u(FE)/δ_u(test)
Test	501.5	33.2	–	–
FE, Ceccotti et al. [47]	500.9	33.4	1.00	1.01
Developed FE	495.3	34.8	0.99	1.05

Table 4
Dimensions and geometrical properties of 3-layered composite beams tested by Zabihi et al. [48] and Ferrier et al. [49].

Beam & Reference	l (m)	a (m)	Layer	Main material	Reinfor. material	$b \times h$ (mm × mm)	Bar (mm^2)
U8-01 & U8-03 [48]	8.0	2.67	2	Timber	–	600 × 35	–
			1	Timber	–	(2 ×)45 × 270	–
			3	Timber	–	(2 ×)140 × 35	–
BLCHP-S-130-5m [49]	5.1	1.70	2	Concrete	Steel	130 × 38	–
			1	Timber	–	130 × 266	–
			3	Concrete	Steel	130 × 42	942

Table 5
Adopted material properties of 3-layered composite beams tested by Zabihi et al. [48] and Ferrier et al. [49].

Beam & Reference	Lay.	Main material					Reinforcement		
		E (GPa)	f_{cu} (MPa)	f_{tu} (MPa)	G_f (MPa)	ε_{c0} (%)	E (GPa)	f_y (MPa)	f_u (MPa)
U8-01 & U8-03 [48]	2	10.7	42.0	34.0	0.22	0.4	–	–	–
	1	13.7	51.4	37.4	0.2	0.4	–	–	–
	3	13.7	51.4	37.4	0.2	0.4	–	–	–
BLCHP-S-130-5m [49]	2	50.0	150.0	17.0	–	0.3	210	400	600
	1	13.4	50.0	40.0	0.3	0.4	–	–	–
	3	50.0	150.0	17.0	–	0.3	210	400	600

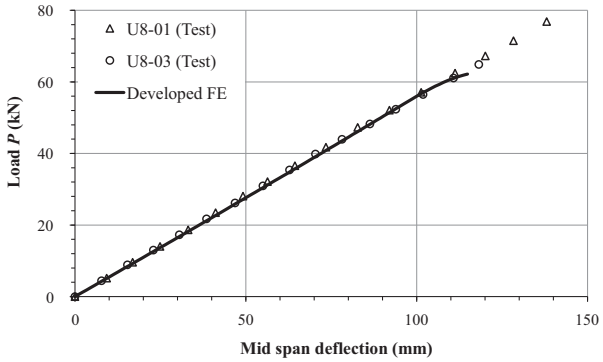

Fig. 17. Load versus midspan deflection of TTC beam tested by Zabihi et al. [48].

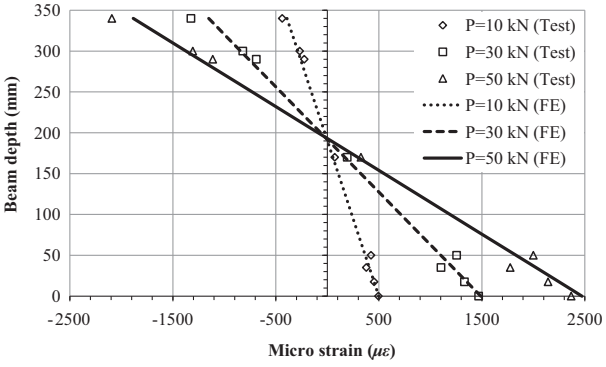

Fig. 18. Strain profile over the beam depth of TTC beam tested by Zabihi et al. [48].

the proposed frame FE model for non-linear short-term analysis of three-layered TCC and TTC composite beams.

6. Conclusions

In this paper a numerical model for non-linear analysis of two- or three-layered composite beams is developed that takes advantage of an efficient 1D frame element with forced-based formulation.

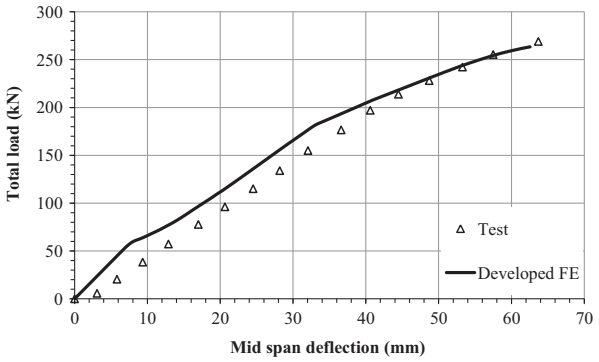

Fig. 19. Total load versus midspan deflection of hybrid beam made of glulam and ultra-high performance concrete tested by Ferrier et al. [49].

The developed element is equipped with lumped translational springs at the nodal points to model the partial shear interaction between the layers. Also, the proposed FE model can capture the material non-linearities including non-linear behaviour of timber under compression, concrete cracking and yielding of reinforcing steel as well as non-linear shear-slip behaviour of connections between the layers. The sections of frame element are discretised into fibres (integration points) and the stiffness matrix of each section can be determined by integrating the stiffness of fibres over the section depth based on Navier–Bernoulli hypothesis. The separation of the layers (vertical interaction) is ignored.

The accuracy and convergence characteristic of the developed FE model with respect to number of elements is studied and the minimum and maximum errors are found to be, respectively, belonging to composite beams with zero and infinite stiffness for the connections. It is also concluded that the frame element developed in this paper has a good convergence rate when the number of elements increase, provided that at least 6 elements are used in the case of composite beams with stiff connections (near full composite action).

The superior performance of the developed FE model for capturing the behaviour of TCC and TTC beams was demonstrated by comparing the numerically predicted results with experimental data. The proposed model can efficiently capture the global response

Table 6
Ultimate loading capacity (P_u) and corresponding ultimate deflection (δ_u) of 3-layered composite beams tested by Zabihi et al. [48] and Ferrier et al. [49].

Beam & Reference	Test		FE		Comparison	
	P_u (kN)	δ_u (mm)	P_u (kN)	δ_u (mm)	P_u(FE)/P_u(test)	δ_u(FE)/δ_u(test)
U8-01 & U8-03 [48]	70.9	128.1	62.2	114.9	0.88	0.90
BLCHP-S-130-5m [49]	269.0	63.7	263.3	62.6	0.98	0.98

(i.e. load versus deflection, slip, strain and stress) of the composite beams up to failure point with reasonable accuracy. Accordingly, the proposed formulation has good potential for analysis of TCC and TTC beams particularly when the time-consuming procedures such as design oriented parametric studies and/or long-term coupled analysis (thermo-hygro-mechanical analysis) are required. It should be noted that coupling of two ordinary frame elements (6 DoFs in each element) by rotational and translational springs leads to a compound element with 12 DoFs, whereas the proposed composite element with two layers has 8 DoFs. This can significantly reduce the computational time.

Acknowledgments

The authors wish to gratefully acknowledge the financial support of the Structural Timber Innovation Company (STIC) Research Consortium that has enabled this work to be undertaken.

Appendix A

A plane composite frame element AB with three layers, five nodes and ten degrees of freedom (i.e. totally 6 horizontal translations, 2 vertical translations and 2 rotations) is assumed. At each end, two non-linear springs with different stiffness are considered to capture the interlayer shear interaction between the layers. Furthermore, the generalised nodal displacement and force vectors for the unrestrained element are

$$\mathbf{q}=\begin{bmatrix}\mathbf{q}_A & \mathbf{q}_B\end{bmatrix}^{\mathrm{T}}=\begin{bmatrix}q_1 & q_2 & q_3 & q_4 & q_5 & q_6 & q_7 & q_8 & q_9 & q_{10}\end{bmatrix}^{\mathrm{T}} \tag{A1}$$

$$\mathbf{Q}=\begin{bmatrix}\mathbf{Q}_A & \mathbf{Q}_B\end{bmatrix}^{\mathrm{T}}=\begin{bmatrix}Q_1 & Q_2 & Q_3 & Q_4 & Q_5 & Q_6 & Q_7 & Q_8 & Q_9 & Q_{10}\end{bmatrix}^{\mathrm{T}} \tag{A2}$$

The force interpolation matrix, the matrix containing the stiffness of connector at end A and B, vector of section generalised forces and vector of total section forces solely due to element loads at end A can be respectively obtained from

$$\mathbf{b}(x)=\begin{bmatrix}-1 & 0 & 0 & 0 & 0\\ 0 & x & -1 & 0 & 0\\ 0 & 0 & 0 & -1 & 0\\ 0 & 0 & 0 & 0 & -1\end{bmatrix} \tag{A3}$$

$$\mathbf{K}_{CA}=K_{A1}\begin{bmatrix}1 & 0 & -H_1 & -1 & 0\\ -H_1 & 0 & {H_1}^2 & H_1 & 0\\ -1 & 0 & H_1 & 1 & 0\\ 0 & 0 & 0 & 0 & 0\end{bmatrix}+K_{A2}\begin{bmatrix}1 & 0 & -H_2 & 0 & -1\\ -H_2 & 0 & {H_2}^2 & 0 & H_2\\ 0 & 0 & 0 & 0 & 0\\ -1 & 0 & H_2 & 0 & 1\end{bmatrix} \tag{A4}$$

$$\mathbf{K}_{CB}=K_{B1}\begin{bmatrix}1 & 0 & -H_1 & -1 & 0\\ -H_1 & 0 & {H_1}^2 & H_1 & 0\\ -1 & 0 & H_1 & 1 & 0\\ 0 & 0 & 0 & 0 & 0\end{bmatrix}+K_{B2}\begin{bmatrix}1 & 0 & -H_2 & 0 & -1\\ -H_2 & 0 & {H_2}^2 & 0 & H_2\\ 0 & 0 & 0 & 0 & 0\\ -1 & 0 & H_2 & 0 & 1\end{bmatrix} \tag{A5}$$

$$\mathbf{D}(x)=\begin{bmatrix}N_1(x) & M(x) & N_2(x) & N_3(x)\end{bmatrix}^{\mathrm{T}} \tag{A6}$$

$$\mathbf{D}_A^*(x)=\begin{bmatrix}N_1^*(x) & M^*(x) & N_2^*(x) & N_3^*(x)\end{bmatrix}^{\mathrm{T}} \tag{A7}$$

where H_1 represents the distance between the mid-planes of the layers 1 and 2; H_2 is the distance between layers 1 and 3; K_{A1} and K_{B1} are the stiffness of the connectors between layers 1 and 2 at end A and B, respectively; K_{A2} and K_{B2} are the stiffness of the connectors between layers 1 and 3 at end A and B, respectively.

Equilibrium over the section yields

$$\mathbf{D}(x)=\begin{bmatrix}\int_{\Omega_1}\sigma_{x1}\,dA\\ -\int_{\Omega_1}\sigma_{x1}y_1\,dA-\int_{\Omega_2}\sigma_{x2}y_2\,dA-\int_{\Omega_3}\sigma_{x3}y_3\,dA\\ \int_{\Omega_2}\sigma_{x2}\,dA\\ \int_{\Omega_3}\sigma_{x3}\,dA\end{bmatrix} \tag{A8}$$

where Ω_i denotes the layer i, y is the distance of the fibre (filament) from the mid-plane of the layer, σ_x is the total stress at the monitoring point within section x along the member axis. The subscripts 1, 2 and 3 denote the component of the corresponding layer.

The secant stiffness matrix of the cross-section, the residual plastic force vector for the section and the section generalised strain vector can, respectively, be obtained from

$$\mathbf{k}_s(x)=\begin{bmatrix}k_{1_{11}} & k_{1_{12}} & 0 & 0\\ k_{1_{12}} & k_{1_{22}}+k_{2_{22}}+k_{3_{22}} & k_{2_{12}} & k_{3_{12}}\\ 0 & k_{2_{12}} & k_{2_{11}} & 0\\ 0 & k_{3_{12}} & 0 & k_{3_{11}}\end{bmatrix} \tag{A9}$$

$$\mathbf{D}_p(x)=\begin{bmatrix}N_{p1}(x) & M_{p1}(x)+M_{p2}(x)+M_{p3}(x) & N_{p2}(x) & N_{p3}(x)\end{bmatrix}^{T} \tag{A10}$$

$$\mathbf{d}(x)=\begin{bmatrix}\varepsilon_{r1} & \varphi & \varepsilon_{r2} & \varepsilon_{r3}\end{bmatrix}^{T} \tag{A11}$$

The transformation matrices are

$$\mathbf{\Gamma}=\begin{bmatrix}-1 & 0 & 0 & 0 & 0\\ 0 & -1 & 0 & 0 & 0\\ 0 & l & -1 & 0 & 0\\ 0 & 0 & 0 & -1 & 0\\ 0 & 0 & 0 & 0 & -1\end{bmatrix} \tag{A12}$$

$$\mathbf{T}=\begin{bmatrix}1 & 0 & 0 & 0\\ 0 & 0 & 0 & 0\\ 0 & 1 & 0 & 0\\ 0 & 0 & 1 & 0\\ 0 & 0 & 0 & 1\end{bmatrix} \tag{A13}$$

The rest of the formulation is similar to the aforementioned two-layered beam and the governing equation of the element is the same as Eq. (36). It is noteworthy that the transformation matrix $\mathbf{\Gamma}$ is directly obtained from the equilibrium equations of the undeformed configuration and this implicitly account for rigid body motion.

References

[1] E. Bou Saïd, J.F. Jullien, A. Ceccotti, Long term modelling of timber–concrete composite structures in variable climates, in: Proceedings of the 8th World Conference on Timber Engineering (WCTE), Lahti, Finland, 2004, p. 6.

[2] A.M.P.G. Dias, et al., A non-linear 3D FEM model to simulate timber-concrete joints, Adv. Eng. Softw. 38 (8–9) (2007) 522–530.

[3] R.M. Gutkowski, J. Balogh, L.G. To, Finite-element modeling of short-term field response of composite wood–concrete floors/decks, J. Struct. Eng. 136 (6) (2010) 707–714.

[4] M. Fragiacomo, A finite element model for long-term analysis of timber–concrete composite beams, Struct. Eng. Mech. 20 (2) (2005) 173–190.

[5] M. Fragiacomo, A. Ceccotti, Long-term behavior of timber–concrete composite beams. I: finite element modeling and validation, J. Struct. Eng. 132 (1) (2006) 13–22.

[6] E. Lukaszewska, M. Fragiacomo, H. Johnsson, Laboratory tests and numerical analyses of prefabricated timber–concrete composite floors, J. Struct. Eng. 136 (1) (2010) 46–55.

[7] M. Heinisuo, An exact finite element technique for layered beams, Comput. Struct. 30 (3) (1988) 615–622.

[8] C. Faella, E. Martinelli, E. Nigro, Steel and concrete composite beams with flexible shear connection: “exact” analytical expression of the stiffness matrix and applications, Comput. Struct. 80 (11) (2002) 1001–1009.

[9] Y. Wu, D.J. Oehlers, M.C. Griffith, Partial-interaction analysis of composite beam/column members, Mech. Struct. Mach. 30 (3) (2002) 309–332.

[10] R. Seracino, et al., Partial interaction stresses in continuous composite beams under serviceability loads, J. Constr. Steel Res. 60 (10) (2004) 1525–1543.

[11] U.A. Girhammar, D.H. Pan, Exact static analysis of partially composite beams and beam-columns, Int. J. Mech. Sci. 49 (2) (2007) 239–255.

[12] B. Jurkiewiez, S. Buzon, J. Sieffert, Incremental viscoelastic analysis of composite beams with partial interaction, Comput. Struct. 83 (21) (2005) 1780–1791.

[13] G. Ranzi, M. Bradford, Analytical solutions for the time-dependent behaviour of composite beams with partial interaction, Int. J. Solids Struct. 43 (13) (2006) 3770–3793.

[14] Q. Nguyen, M. Hjiaj, B. Uy, Time-dependent analysis of composite beams with continuous shear connection based on a space-exact stiffness matrix, Eng. Struct. 32 (9) (2010) 2902–2911.

[15] A. Ayoub, F.C. Filippou, Mixed formulation of nonlinear steel–concrete composite beam element, J. Struct. Eng. 126 (3) (2000) 371–381.

[16] E. Spacone, S. El-Tawil, Nonlinear analysis of steel–concrete composite structures: state of the art, J. Struct. Eng. 130 (2) (2004) 159–168.

[17] L. Macorini, et al., Long-term analysis of steel–concrete composite beams: FE modelling for effective width evaluation, Eng. Struct. 28 (8) (2006) 1110–1121.

[18] A. Saritas, F.C. Filippou, Inelastic axial-flexure–shear coupling in a mixed formulation beam finite element, Int. J. Non-Linear Mech. 44 (8) (2009) 913–922.

[19] A. Heidarpour, M.A. Bradford, Generic non-linear modelling of a bi-material composite beam with partial shear interaction, Int. J. Non-Linear Mech. 44 (3) (2009) 290–297.

[20] N. Challamel, On geometrically exact post-buckling of composite columns with interlayer slip—the partially composite elastica, Int. J. Non-Linear Mech. 47 (3) (2012) 7–17.

[21] M. Hjiaj, J.-M. Battini, Q. Huy Nguyen, Large displacement analysis of shear deformable composite beams with interlayer slips, Int. J. Non-Linear Mech. 47 (8) (2012) 895–904.

[22] N. Xiao, H. Zhong, Non-linear quadrature element analysis of planar frames based on geometrically exact beam theory, Int. J. Non-Linear Mech. 47 (5) (2012) 481–488.

[23] B.L. Deam, M. Fragiacomo, A.H. Buchanan, Connections for composite concrete slab and LVL flooring systems, Mater. Struct. 41 (3) (2008) 495–507.

[24] A. Ceccotti, M. Fragiacomo, S. Giordano, Long-term and collapse tests on a timber–concrete composite beam with glued-in connection, Mater. Struct. 40 (1) (2006) 15–25.

[25] D. Yeoh, et al., Experimental tests of notched and plate connectors for LVL–concrete composite beams, J. Struct. Eng. 137 (2) (2011) 261–269.

[26] J. Aribert, K. Abdel Aziz, Calcul des poutres mixtes jusqu'à l'état ultime avec un effet de soulèvement à l'interface acier-béton, Constr. Met. 4 (1985) 3–36.

[27] H. Robinson, K. Naraine., Slip and uplift effects in composite beams, in: International Conference on Composite Construction in Steel and Concrete. Proceedings of Engineering Foundation Conference on Composite Construction, ASCE, Henniker, New Hampshire, (1988) pp. 487–497.

[28] Q.-H. Nguyen, M. Hjiaj, S. Guezouli, Exact finite element model for shear-deformable two-layer beams with discrete shear connection, Finite Elem. Anal. Des. 47 (7) (2011) 718–727.

[29] S. Schnabl, I. Planinc, The effect of transverse shear deformation on the buckling of two-layer composite columns with interlayer slip, Int. J. Non-Linear Mech. 46 (3) (2011) 543–553.

[30] A. Yasunori, H. Sumio, T. Kajita, Elastic–plastic analysis of composite beams with incomplete interaction by finite element method, Comput. Struct. 14 (5) (1981) 453–462.

[31] G. Ranzi, M.A. Bradford, Analysis of composite beams with partial interaction using the direct stiffness approach accounting for time effects, Int. J. Numer. Methods Eng. 78 (5) (2009) 564–586.

[32] A. Zona, G. Ranzi, Finite element models for nonlinear analysis of steel–concrete composite beams with partial interaction in combined bending and shear, Finite Elem. Anal. Des. 47 (2) (2011) 98–118.

[33] G. Ranzi, Locking problems in the partial interaction analysis of multi-layered composite beams, Eng. Struct. 30 (10) (2008) 2900–2911.

[34] J.B.M. Sousa , A.R. da Silva, Analytical and numerical analysis of multilayered beams with interlayer slip, Eng. Struct. 32 (6) (2010) 1671–1680.

[35] L. Škec, et al., Analytical modelling of multilayer beams with compliant interfaces, Struct. Eng. Mech. 44 (4) (2012) 465–485.

[36] D. Zabulionis, O. Kizinievič, L. Feo, An analysis of the stress–strain state of a timber-concrete T cross section, Composites Part B: Eng. 45 (1) (2013) 148–158.

[37] H.R. Valipour, M.A. Bradford, A steel–concrete composite beam element with material nonlinearities and partial shear interaction, Finite Elem. Anal. Des. 45 (12) (2009) 966–972.

[38] A. Saritas, O. Soydas, Variational base and solution strategies for non-linear force-based beam finite elements, Int. J. Non-Linear Mech. 47 (3) (2012) 54–64.

[39] S. Schnabl, et al., An analytical model of layered continuous beams with partial interaction, Struct. Eng. Mech. 22 (3) (2006) 263–278.

[40] J.B.M. Sousa , Exact finite elements for multilayered composite beam-columns with partial interaction, Comput. Struct. (2013) 48–57123 (2013) 48–57.

[41] H. Murakami, A laminated beam theory with interlayer slip, J. Appl. Mech. (Trans. ASME) 51 (3) (1984) 551–559.

[42] J. Bareisis, Stiffness and strength of multilayer beams, J. Compos. Mater. 40 (6) (2006) 515–531.

[43] H.R. Valipour, S.J. Foster, Nonlocal damage formulation for a flexibility-based frame element, J. Struct. Eng. 135 (10) (2009) 1213–1221.

[44] T.E. Conners, Segmented models for stress-strain diagrams, Wood Sci. Technol. 23 (1) (1989) 65–73.

[45] P. ,Glos, Zur Modellierung des Festigkeitsverhaltens von Bauholz bei Druck-, Zug- und Biegebeanspruchung, in: Berichte zur Zuverlässigkeitstheorie der Bauwerke, SFB 96: Munich, Germany, 1981.

[46] CEB-FIP, CEB-FIP model code 1990: Design code, Thomas Telford, London, 1993.

[47] A. Ceccotti,M. Fragiacomo, S. Giordano, Behaviour of a timber–concrete composite beam with glued connection at strength limit state, in: Proceedings of the 9th World Conference on Timber Engineering (WCTE), 2006, Portland, OR, USA, p. 8.

[48] Z. Zabihi,et al., Serviceability and ultimate performance of long span timber floor modules, in: Proceedings of the 12th World Conference on Timber Engineering (WCTE), Auckland, New Zealand, 2012, pp. 378–385.

[49] E. Ferrier, P. Labossìre, K.W. Neale, Mechanical behavior of an innovative hybrid beam made of glulam and ultrahigh-performance concrete reinforced with FRP or Steel, J. Compos. Constr. 14 (2) (2010) 217–223.

[50] E. Ferrier, P. Labossière, K.W. Neale, Modelling the bending behaviour of a new hybrid glulam beam reinforced with FRP and ultra-high-performance concrete, Appl. Math. Model. 36 (8) (2012) 3883–3902.